

Isolation, Characterization, Molecular Docking, and Antimalarial Activity of Chemical Constituents of *Diospyros adenophora*.

Ibrahim Dankane Bafarawa^{1,2}, Muhammad Solehin Abd Ghani¹, Mohamad Nurul Azmi^{1*}, Arba Pramundita Ramadani³, Dian Nida Salsabila³, Arde Toga Nugraha³, Sista Werdyani³, Muhammad Bisyrul Hafi Othman¹, Mohammad Nasir Ibrahim¹, Khalijah Awang⁴, Marc Litaudon⁵, and Mohammad Tasyriq Che Omar⁶

¹School of Chemical Sciences, Universiti Sains Malaysia, 11800 Penang, Malaysia

²Umaru Ali Shinkafi Polytechnic Sokoto, P.M.B. 2356 Sokoto State, Nigeria

³Department of Pharmacy, Universitas Islam Indonesia, Jl. Kaliurang KM 14.4 Sleman, Yogyakarta 55584, Indonesia

⁴Department of Chemistry, Faculty of Science, University of Malaya, 50603 Kuala Lumpur, Malaysia

⁵Institute de Chimie des Substances Naturelles, CNRS-ICSN UPR2301, Univ. Paris-Sud 11, av. de la Terrasse, 91198 Gif-sur-Yvette, France

⁶Biological Section, School of Distance Education, Universiti Sains Malaysia, 11800 Minden, Penang, Malaysia

*Corresponding author (e-mail: mnazmi@usm.my)

Malaria remains the number one killer disease publicly, leading to the search for a new potent agent that fights against *plasmodial falciparum*. *Diospyros Adenophora* (Ebenaceae) is a shrub or tree grown primarily in the wet tropical biome including Peninsula Malaysia. The species of *Diospyros* have been reported to exhibit interesting biological properties such as antimalaria. Interestingly, no scientific report was documented on the species *D. adenophora*. In the present study, three known pentacyclic triterpenoids namely lupenone (**1**), lupeol (**2**), and betulin (**3**) were isolated from this species and fully characterized using extensive spectroscopic data like 1D- and 2D- nuclear magnetic resonance (NMR) as well as FT-IR and HRESIMS and subsequently compared with the reported literature. All compounds were screened *in vitro* for anti-malarial activity against β -hematin polymerization inhibition as well as molecular docking. The *in vitro* analysis revealed that compound **2** is the most active, with an IC₅₀ value of 20.2 ± 17 μ M, followed by compound **1** having an IC₅₀ value of 27.5 ± 23 μ M. These compounds have a lower IC₅₀ value than chloroquine (37.5 ± 0.6 μ M) as a control. Compound **3** exhibits moderate activity (IC₅₀: 40.9 ± 22 μ M) in comparison to the control. In addition, all compounds displayed high binding energy in comparison to standard chloroquine (-7.7 kcal/mol), as determined by molecular docking data. The total binding energy of lupenone (**1**) and betulin (**3**) with hemozoin crystal is -8.6 and -9.2 kcal/mol, respectively. While lupeol (**2**) was observed to have a high binding energy at -9.7 kcal/mol, it is considered the best binding interaction with hemozoin crystal. Based on the results obtained from *in vitro* β -hematin polymerization inhibition and the *in-silico* analysis, compounds **1** and **2** are predicted to be potential anti-malarial agents.

Keywords: *Diospyros adenophora*; Ebenaceae; triterpenoids; anti-malarial activity, β -hematin inhibitor

Received: September 2023; Accepted: November 2023

Malaria is the most dangerous blood-borne protozoan disease caused by *Plasmodium* parasites which is transmitted to human being through the bites of infected female *Anopheles* mosquitos [1]. Despite living in a time of tremendous technology, and advances in the control and prevention of diseases, malaria continues to be one of the major transmissible and deadly diseases in the world [2]. The incidence of malaria is increasing every year with approximately 300 million new cases reported annually, resulting in about one million deaths annually, with children below five years accounting for 75 per cent of these

fatalities [3]. The rapid emergence and spread of resistant strains throughout endemic areas is the major problem with malaria. Artemisinin-based combination therapies (ACTs) are the most reliable, genuine, and effective anti-malaria drugs [4]. Sadly, the emergence of drug resistance to artemisinin and artesunate components of the multiple ACTs and the non-artemisinin-based combination therapy rendered the instrument ineffective [5]. Therefore, finding novel effective, and non-drug-resistant antimalarial agents from natural resources is needed. Indeed, the *Plasmodium* parasite digests hemoglobin in vacuole

into amino acids and heme. Hence, the best strategy to control malaria diseases is by detoxification its mechanisms such as hemozoin formation, degradation of free heme by H₂O₂, and heme-binding proteins [1].

Natural products have demonstrated themselves as a significant source of novel drugs including antimalarial agents since the discovery of the first antimalarial drug in the 1800s [6]. Indeed, plant-based remedies are used as first-line treatment for various diseases and disorders [7]. In this regard, *Diospyros adenophora* (*D. adenophora*) is among the family of Ebenaceae with no scientific evidence recorded yet. This plant is native to Malaysia and belongs to the *Diospyros* genus with more than 500 species. Their evergreen shrubs and trees are distributed in the tropical and subtropical regions of the world [8]. This genus has great promising health benefits with incredible economic values [9]. Various chemical constituents have been isolated from the species of this genus, such as triterpenes, naphthoquinones, steroids, flavonoids, and phenolic acids [8, 10, 11]. The active compounds isolated from the species of this genus have demonstrated interesting biological applications like anti-analgesic and anti-inflammatory activity [12], cytotoxic activity [13], antimicrobial activity [14], relief of pain and fever [15], anti-oxidant activity [16], anthelmintic activity [17], antiadipogenic hypolipidemic, antidiabetic activity [18], antiproliferative activity [19], and anti-malarial activity [7]. Thus, exploring the chemistry and the anti-malarial activity of *D. Adenophora* could be an initial step to unravel the potential of this virgin plant.

Therefore, in this study, the chemical constituents from the *D. adenophora* were isolated, characterized and evaluated through *in vitro* anti-malarial activity on β -hematin polymerization inhibition and molecular docking study. This plant is a new species, and this is the first report on chemical constituents from this plant with their biological activity.

EXPERIMENTAL

Chemicals and Materials

All chemical reagents and solvents such as *n*-hexane, dichloromethane, ethyl acetate, methanol, chloroform-D1, vanillin, and sulphuric acids (AR grades) were obtained from QR&C (Asia) and Merck (Germany) and used without further purification. Normal column chromatography (CC) was employed to separate fractions using silica gel 60 of 70-230 and 230-400 mesh (Merck, Germany) as the stationary phase depending on the weight of the crude or fractions. To distinguish the presence of compounds in the extracts thin-layer chromatography (TLC) was carried out on alumina plates pre-coated with silica gel 60 F₂₅₄ plates (Merck, Germany). Spots of compounds were visualized on TLC plates, using vanillin-sulphuric acid vapor as a detecting reagent.

Instrumentations

All spectral data were analyzed by spectroscopic instrument. Fourier-transform Infrared was recorded using Perkin Elmer ATR FT-IR spectrometer in the 600-4000 cm⁻¹ range. Also, FT-NMR Bruker Advance 500 (500 MHz for ¹H-NMR, 125 MHz for ¹³C-NMR) spectrometer was used to record 1D- and 2D-nuclear magnetic resonance (NMR) spectra in CDCl₃ (¹H: 7.26 ppm and ¹³C: 77.0 ppm) using tetramethyl silane (TMS) as internal standard (Bruker Bioscience, Billerica, Massachusetts, USA). Topspin 3.6.2 software package was used to analyze the data. Chemical shifts are recorded in parts per million (ppm), and coupling constants, *J* are presented in Hertz (Hz). The HRMS analysis of the compounds was recorded with a water xevo QTOF MS spectrometer, the data obtained are reported in *m/z*. The TLC plates were examined using a UV radiation lamp (max = 254 and 365 nm) and vanillin-sulphuric acid were used to visualize the spots. Melting points were determined on open capillary tubes and using Stuart SMP-10 apparatus.

Plant Material

The bark of *D. adenophora* with code number KL5430B was collected in June 2007 at the Reserved Forest of Madek, Lenggong, Keluang, Johor, Malaysia. The specimen was identified by the botanist Teo L.E., from the University of Malaya. Afterward, the voucher specimen was stored at the Herbarium of the Chemistry Department, Faculty of Science, University of Malaya, Kuala Lumpur, Malaysia.

Extractions and Isolations

The dry bark of *D. adenophora* (0.6 kg) was immersed in 3.0 L ethyl acetate (EtOAc) at room temperature for 4 days, to allow the solvent to extract the soluble molecule within their polarity. The process was repeated 2 times consecutively using fresh ethyl acetate solvent. The extracts were filtered on a No.1 Whatman filter paper, and the filtrates were evaporated using a rotary evaporator under a reduced pressure of a temperature below 40°C to attain the EtOAc crude extracts. The residue was then immersed in 3.0 L of methanol (MeOH) by following a similar method above. The crude methanol extracts were kept for future use. The crude ethyl acetate extracts 7.0 g were subjected to normal column chromatography over a silica gel 60 (70-230 mesh) eluted with *n*-hexane/EtOAc (100:0 → 20:80) step gradient solvent system, yielded 11 sub-fractions denoted as DA1 to DA11. Based on the thin layer chromatography (TLC) profile, DA1 to DA11 was further subjected to purification using column chromatography eluting *n*-hexane/EtOAc (100:0 → 20:80) step gradient solvent system. Purification of DA1 using column chromatography technique yielded compound **1** at solvent system *n*-hexane/EtOAc (95:5). Meanwhile, DA1-DA11 was combined (based on their similarity in the thin layer chromatography (TLC)

profile) and purified by same method above with gradient system of increasing polarity *n*-hexane/EtOAc (90:10 → 80:20), afforded compounds **2** and **3**. The structure of the compounds were determined using spectroscopic technique and compared with those of authentic samples and with published data [20-22]. These compounds were identified namely lupenone (**1**), lupeol (**2**), and betulin (**3**), respectively.

Lupenone (1): Brown oil; Yield: 0.13 g (0.02 %); FT-IR (ATR) ν_{\max} cm^{-1} : 2939 (Csp²-H), 2849 (Csp³-H), 1722 (C=O), 1643 (C=C); HRESIMS (+ESI) [M+Na]⁺: 447.3605, C₃₀H₄₈ONa, requires 447.3603; ¹H-NMR (CDCl₃), 1.19 (m, H-1), 2.47 (m, H-2), 0.77 (m, H-5), 1.47 (m, H-6), 1.44 (H-7), 1.29 (m, H-9), 1.41 (m, H-11), 1.65 (m, H-12), 1.66 (m, H-13), 1.70 (m, H-15), 1.48 (m, H-16), 1.40 (m, H-18), 2.38 (m, H-19), 1.28, 1.93 (m, H-21), 1.19, 1.39 (m, H-22), (1.25 (s, H-23), 1.02 (s, H-24), 1.07 (s, H-25), 0.93 (s, H-26), 0.96 (s, H-27), 0.79 (s, H-28), 4.59, 4.68 (H-29), 1.67 (H-30); ¹³C-NMR . 39.7 (C-1), 34.3 (C-2), 218.1 (C-3), 47.4 (C-4), 55.1 (C-5), 19.5 (C-6), 33.8 (C-7), 40.8 (C-8), 49.9 (C-9), 37.0 (C-10), 21.6 (C-11), 25.3 (C-12), 38.3 (C-13), 43.0 (C-14), 27.5 (C-15), 35.7 (C-16), 43.1 (C-17), 48.4 (C-18), 48.1 (C-19), 150.1 (C-20), 29.9 (C-21), 40.1 (C-22), 26.7 (C-23), 21.1 (C-24), 15.9 (C-25), 16.0 (C-26), 14.6 (C-27), 18.1 (C-28), 109.5 (C-29), 17.8 (C-30).

Lupeol (2): White powder; Yield: 0.97 g (0.16 %); M.p.: 219–221 °C; FT-IR (ATR) ν_{\max} cm^{-1} : 3307 (O-H), 2936 (Csp²-H), 2861 (Csp³-H), 1647 (C=C); HRESIMS (+ESI) [M+H]⁺: 427.3927, C₃₀H₅₁O, requires 427.3939; ¹H-NMR (CDCl₃), 0.91 (m, H-1), 1.59, 1.65 (m, H-2), 3.18 (dd. $J_1=5.1$, $J_2=11.5$, H-3), 0.67 (d. $J=9.5$, H-5), 1.38, 1.51 (m, H-6), 1.38 (m, H-7), 1.26 (m, H-9), 1.41 (m, H-11), 1.65 (m, H-12), 1.64 (m, H-13), 1.65 (m, H-15), 1.36, 1.47 (m, H-16), 1.36 (m, H-18), 2.38 (m, H-19), 1.30, 1.91 (m, H-21), 1.37, 1.19 (m, H-22), 0.97 (s, H-23), 0.76 (s, H-24), 0.82 (s, H-25), 1.03 (s, H-26), 0.93 (s, H-27), 0.79 (s, H-28), 4.58, 4.67 (H-29), 1.67 (s, H-30). ¹³C-NMR, 38.9 (C-1), 27.5 (C-2), 79.1 (C-3), 39.0 (C-4), 55.5 (C-5), 18.5 (C-6), 34.4 (C-7), 41.1 (C-8), 50.6 (C-9), 37.3 (C-10), 21.1 (C-11), 25.3 (C-12), 38.2 (C-13), 43.0 (C-14), 27.6 (C-15), 35.8 (C-16), 43.1 (C-17), 48.5 (C-18), 48.1 (C-19), 151.0 (C-20), 30.0 (C-21), 40.1 (C-22), 28.1 (C-23), 15.5 (C-24), 16.2 (C-25), 16.1 (C-26), 14.7 (C-27), 18.1 (C-28), 109.5 (C-29), 19.4 (C-30).

Betulin (3): White powder; Yield: 1.75 g (0.29 %); M.p.: 242–246 °C; FT-IR(ATR) ν_{\max} cm^{-1} : 3357 (O-H), 2939 (Csp²-H), 2867 (Csp³-H), 1643 (C=C); HRESIMS (+ESI) [M+Na]⁺: 465.3709, C₃₀H₅₀O₂Na, requires 465.3708; ¹H-NMR (CDCl₃), 0.88 (dd. $J_1=5.1$, $J_2=12.5$, H-1), 1.59, 1.64 (m, H-2), 3.20 (dd. $J_1=5.0$, $J_2=11.5$, H-3), 0.69 (d. $J=10.0$, H-5), 1.39, 1.53 (m, H-6), 1.39 (m, H-7), 1.25 (m, H-9), 1.21, 1.42 (m, H-11), 1.05, 1.65 (m, H-12), 1.61 (m, H-13), 1.65, 1.70 (m, H-15), 1.28, 1.91 (m, H-16), 1.59 (m, H-18), 2.38 (m, H-19), 1.26, 1.96 (m, H-21), 1.03, 1.85 (m,

H-22), 0.97 (s, H-23), 0.75 (s, H-24), 0.83 (s, H-25), 1.02 (s, H-26), 0.98 (s, H-27), 3.33 (d. $J=11.2$, H-28), 4.58, 4.68 (H-29), 1.68 (s, H-30). ¹³C-NMR, 38.9 (C-1), 27.5 (C-2), 79.2 (C-3), 39.0 (C-4), 55.5 (C-5), 18.5 (C-6), 34.4 (C-7), 41.1 (C-8), 50.5 (C-9), 37.3 (C-10), 20.9 (C-11), 25.2 (C-12), 37.3 (C-13), 42.9 (C-14), 27.2 (C-15), 29.2 (C-16), 47.9 (C-17), 48.9 (C-18), 47.9 (C-19), 150.3 (C-20), 29.8 (C-21), 34.2 (C-22), 28.2 (C-23), 15.5 (C-24), 16.2 (C-25), 16.1 (C-26), 14.9 (C-27), 60.8 (C-28), 109.8 (C-29), 19.2 (C-30).

β -Hematin Polymerization Inhibition

The β -hematin polymerization inhibition assay was conducted *in vitro* for three compounds namely lupenone (**1**), lupeol (**2**), and betulin (**3**) based on [21], method with slight modifications. As much as 100 μL of 1 mM hematin solution in 0.2 M NaOH was mixed with the various concentrations of the test compounds (14.1, 28.2, 56.5, 112.9, and 225.9 μM consecutively) in a microtube. Samples of each concentration was prepared in triplicate with 10% DMSO as a control and chloroquine as a drug reference. The polymerization reaction was started with the addition of 50 μL glacial acetic acid (pH 2.6) into a hematin-contained microtube, followed by incubation for 24 hours at 37°C. At the end of the incubation period, the tube was centrifuged at 8000 rpm for 10 minutes, and the precipitate (the hematin crystal) was collected three times washing using 200 μL of DMSO. The final precipitate was then dissolved with 200 μL of 0.1 M NaOH and 100 μL of the solution was transferred to a 96-well microplate. The plate was read using the ELISA Reader at 405 nm. A standard curve was composed to represent the relationship between hematin concentrations (range from 9 to 150 μM) and their absorbance for quantifying the amount of β -hematin concentration of each well. A different standard curve was created for each experiment.

Statistical Analysis

The β -hematin polymerization inhibition activity was expressed in IC₅₀ values determined by Probit analysis using IBM SPSS version 25.

Molecular Docking Studies

Molecular docking is a computational technique for predicting the preferred orientation of a molecule (ligand) when it binds to a molecular target (receptor). Docking contributes to the understanding of ligand-receptor interactions and provides insights into binding affinities, interaction energies and active site preferences, which facilitates drug research and development [24]. In this study, the molecular docking was performed using the AutoDock Vina [25, 26] tools in UCSF Chimera program 1.17.3 (Regents of University of California, CA, USA). The structures of the isolated compounds, identified as ligands were constructed using ChemDraw Professional 22.00 software (Perkin

Elmer Informatics, MA, USA). Next, Chem3D tools of ChemDraw software was employed to convert the ligands into the three-dimensional (3D) structures. The energy was minimized using MM2 force field and then saved into a protein data bank (.pdb) format. The ligands underwent additional processing in UCSF Chimera using Dock Prep tools. This involved tasks such as adding polar hydrogens and Gasteiger partial charges, consolidating non-polar hydrogen atoms, and specifying rotatable bonds, ultimately transforming the .pdb file into .pdbqt format. Next, the crystal structure of β -hematin was retrieved from Cambridge Crystallographic Data Centre (CCDC) (CCDC number: XETXUP01) [27]. Using the VESTA software developed by Momma and Izumi in 2011, the crystal structure of β -hematin was converted into a hemozoin supercell matrix with a $2 \times 2 \times 2$ crystal lattice and subsequently saved in .pdb format. Afterward, polar hydrogens were introduced, non-polar hydrogens were fused, the solvation parameter was incorporated, and Kollman charges were assigned to the hemozoin supercell receptor within the Dock Prep tools. The center for docking, situated at coordinates (9.04, 14.05, 8.79) in the x, y, and z dimensions, was established within a grid box measuring $40.0 \text{ \AA} \times 56.0 \text{ \AA} \times 51.0 \text{ \AA}$, encompassing the entire hemozoin receptor. The docking configuration included specifications for 10 binding modes, 8 exhaustive search iterations, and a maximum energy difference threshold of 2 kcal mol^{-1} . Consequently, we acquired 10 ligand models and evaluated them based on the binding energy's potency. Finally, the ligand-receptor model exhibiting the most favorable binding energy was chosen. This selected ligand-receptor model was then scrutinized and represented to visualize their active interactions in 3D conformations using BIOVIA Discovery Studio Visualizer (Dassault Systemes, CA, USA).

RESULTS AND DISCUSSION

Isolation and Structural Elucidation

The EtOAc crude extract was separated by column chromatography over a silica gel to give Fr1 – Fr11 denoted as DA1 to DA11. Based on the TLC profile DA1-DA11 was further subjected to purification using

column chromatography over a silica gel eluting with *n*-hexane/EtOAc step gradient solvent system, yielding three compounds. The structure of the compounds was confirmed by 1D- and 2D-NMR analysis as well as FT-IR and HRESIMS data. The information received from spectroscopic data of the isolated compounds **1-3** compared with reported literature suggested to be triterpenes skeleton.

Compound **1** was isolated as a brownish liquid (0.13 g), with a percentage yield of 0.02%. The FT-IR spectrum indicated some important absorption bands at 2936 ($\text{C}_{\text{sp}^2}\text{-H}$), 2849 ($\text{C}_{\text{sp}^3}\text{-H}$), and 1722 (C=O), also HRESIMS (^+ESI) $[\text{M}+\text{Na}]^+$ showed molecular ion peak at m/z 447.3605 $\text{C}_{30}\text{H}_{48}\text{ONa}$ (Calculated: 447.3603). $^1\text{H-NMR}$ spectrum as shown in Table 1 displayed seven methyl singlets peaks at δ_{H} 1.67, 1.25, 1.07, 1.02, 0.93, 0.96, and 0.79, respectively. In addition, the spectrum also exhibited the appearance of two olefinic protons at δ_{H} 4.57 and 4.68, signifying the characteristic of lupane skeleton peaks. Moreover, the $^{13}\text{C-NMR}$ and DEPT-135 spectrum displayed 30 carbon signals, including signals at δ_{C} 150.1 and 109.5 of one isopropenyl group $-\text{C}(\text{CH}_3)=\text{CH}_2$ corresponding to olefinic carbon at C-20 and C-29, respectively. The signals at δ_{C} 218.1 correspond to the carbonyl carbon peak of C-3. Besides the two quaternary carbons mentioned representing C-20 and C-3, the spectrum also indicates the presence of ten methylene, five methine carbons peaks, and another five quaternary carbons in positions C-4, C-8, C-10, C-14, and C-17, respectively. Furthermore, in the $^1\text{H-}^1\text{H}$ COSY spectrum, there is a correlation between the proton H-2/H-3, then H-1/H-2. Similarly, there is also a correlation between proton H-5/H-6, H-7/H-6, H-9/H-26, and H-22/H-21 respectively. Moreover, the HMBC spectrum displayed inter-correlation peaks between H-1/C-3, H-24/C-23, H-30/C-20, H-30/C-29, H-27/C-15, and H-23/C-3. Additionally, it showed an interconnection between the proton signal of the exocyclic double H-29 and the methyl C-30 of the lupane skeleton as well as the olefinic quaternary C-20. This correlation confirms its lupane skeleton. This information is in accordance with the reported literature [20] and compound **1** was identified as lupenone.

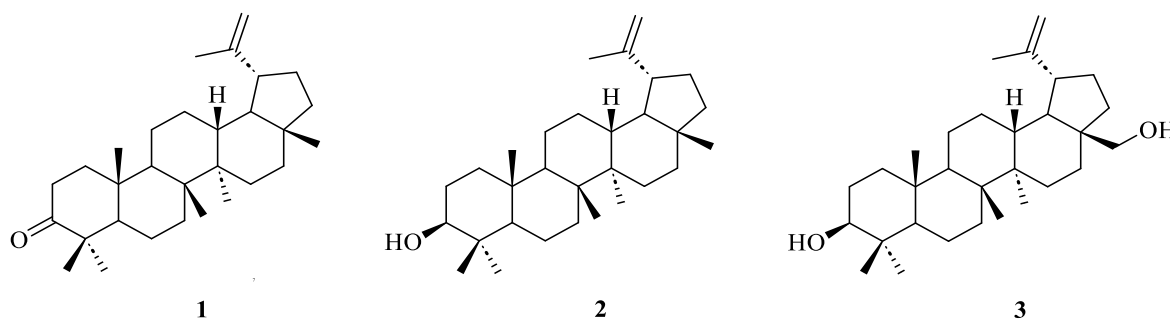


Figure 1. Chemical constituents isolated from *D. adenophora*.

Table 1. ¹H-NMR (in CDCl₃, 500 MHz) and ¹³C-NMR (in CDCl₃, 125 MHz) data of compounds **1–3**.

Position	Compound 1		Compound 2		Compound 3	
	δ_{H} (J in Hz)	δ_{C}	δ_{H} (J in Hz)	δ_{C}	δ_{H} (J in Hz)	δ_{C}
1	1.19 m, 1.38 m	39.7	0.91 m	38.9	0.88 dd (5.1, 12.5)	38.9
2	2.47 m	34.3	1.59 m, 1.65 m	27.5	1.59 m, 1.64 m	27.5
3	-	218.1	3.18 dd (5.1, 11.5)	79.1	3.20 dd (5.0, 11.5)	79.2
4	-	47.4	-	39.0	-	39.0
5	0.77	55.1	0.67 (9.5)	55.5	0.69 d (10.0)	55.5
6	1.47 m, 1.69 m	19.5	1.38 m, 1.51 m	18.5	1.39 m, 1.53 m	18.5
7	1.44	33.8	1.38	34.4	1.39 m	34.4
8	-	40.8	-	41.1	-	41.1
9	1.29 m	49.9	1.26 m	50.6	1.25 m	50.5
10	-	37.0	-	37.3	-	37.3
11	1.41 m	21.6	1.41 m	21.1	1.21 m, 1.42 m	20.9
12	1.65 m	25.3	1.65 m	25.3	1.05 m, 1.65 m	25.2
13	1.66 m	38.3	1.64 m	38.2	1.61 m	37.3
14	-	43.0	-	43.0	-	42.9
15	1.70 m	27.5	1.65 m	27.6	1.65 m, 1.70 m	27.2
16	1.48 m	35.7	1.36 m, 1.47 m	35.8	1.28 m, 1.91 m	29.2
17	-	43.1	-	43.1	-	47.9
18	1.40 m	48.4	1.36 m	48.5	1.59	48.9
19	2.38 m	48.1	2.38 m	48.1	2.38	47.9
20	-	150.1	-	151.0	-	150.3
21	1.28 m, 1.93 m	29.9	1.30 m, 1.91 m	30.0	1.26 m, 1.96 m	29.8
22	1.19 m, 1.39 m	40.1	1.37 m, 1.19 m	40.1	1.03 m, 1.85 m	34.2
23	1.25 s	26.7	0.97 s	28.1	0.97 s	28.2
24	1.02 s	21.1	0.76 s	15.5	0.75 s	15.5
25	1.07	15.9	0.82 s	16.2	0.83 s	16.2
26	0.93 s	16.0	1.03 s	16.1	1.02 s	16.1
27	0.96 s	14.6	0.93 s	14.7	0.98 s	14.9
28	0.79 s	18.1	0.79 s	18.1	3.33 d (10.9) 3.80 d (11.2)	60.8
29	4.57 s, 4.68 s	109.5	4.58 s, 4.67 s	109.5	4.58 s, 4.68 s	109.8
30	1.67 s	19.8	1.67 s	19.4	1.68 s	19.2

(s= singlet, d= doublet, dd=doublet of doublet, m= multiplet)

Compound **2** was obtained as a white powder (0.97 g) with a percentage yield of 0.16 % and a melting point of 219–221 °C. FT-IR showed a peak at 3307 corresponding to the (O-H) group, another significant peak at 2936 assigned to (Csp²-H), and 1647 for (C=C). HRESIMS [M+H]⁺ showed a molecular ion peak at 427.3927 C₃₀H₅₁O (Calculated: 427.3939). The ¹H-NMR spectrum displayed seven angular methyl protons peaks at δ_{H} 0.76, 0.79, 0.82, 0.93, 0.97, 1.03, and 1.67 corresponding H-24, H-28, H-25, H-27, H-23, H-26, and H-30, respectively. Similarly, the proton NMR spectrum indicated a signal at δ_{H} 3.18 as double of doublet, assigned H-3. There is also, the presence of doublets for the geminal protons at δ_{H} 4.67 and 4.58 assigned to H-29a and H-29b indicating that compound **2** was a triterpene derivative. Moreover, the ¹³C-NMR and DEPT-135 as shown in Table 1 indicated 30 carbon signals for the terpenoid of the lupane skeleton. These include seven methyl carbon peaks, six methines, eleven methylene's, and six quaternary carbon peaks. The characteristic of an α -oriented hydrogen of a

3 β -hydroxy triterpene was observed in a carbon bonded to the OH group at the C-3 position that appeared at δ_{C} 79.1. The olefinic carbon peaks of the exocyclic double of the lupane skeleton assigned to C-20 and C-29 were identified at δ_{C} 151.0 and 109.5. Compounds **1** and **2** share similar structure assignments except in position C-3, in which C=O of **1** was replaced by the α -oriented hydrogen of 3 β -hydroxy triterpene in compound **2** shifting the neighbouring protons to a more up-field region. ¹H-¹H COSY assessment showed correlations between H-3/H-2, H-13/H-19, H-6/H-7, H-30/H-29a, H-2/H-1, H-21/H-22, H-7/H-6, and H-18/H-19. Meanwhile, the HMBC spectrum exhibited a correlation between H-19/C-21 and C-29, it also presented a correlation between the proton signal of exocyclic double H-29 with olefinic quaternary C-20 as well as methyl C-30 of lupane skeleton. The proton signal H-3 correlates with carbon assigned C-24 and methylene C-2. Other correlations observed include the proton H-23 with C-3 and proton H-30 with quaternary C-20. The spectroscopic data were compared with the reported

literature [21], and it was confirmed that the isolated compound has the same skeleton as triterpene compounds and was assigned as lupeol.

Compound 3 was isolated as a white powder (1.75 g); with 0.29 % yield and melting point 242–246 °C range. FT-IR showed a broad peak at 3357 indicating the presence of a hydroxyl group (OH) in the compound and another peak at 2939 for (Csp²-H), while the carbon double peak appeared at 1643 corresponding to (C=C). HRESIMS [M+Na]⁺ molecular ion peak was observed at 465.3709 C₃₀H₅₀O₂Na (Calculated: 465.3708). The structural assessment of this compound is the same as that of compounds **1** and **2**. The ¹H-NMR spectrum indicates six methyl protons peak at δ_H 0.75, 0.83, 0.97, 0.98, 1.02, and 1.68. correspond to H-24, H-25, H-23, H-27, H-26, and H-30 respectively, showing it's a triterpenes compound. It also demonstrates the presence of a diastereotopic proton assigned to the methylene group δ_H 3.33 (1H, d, *J* = 10.9 Hz) and δ_H 3.80 (1H, d, *J* = 11.2 Hz) attached to the hydroxyl group at C-28. The signal at δ_H 3.20 (dd, *J* = 5.0, 11.5 Hz) corresponds to α-oriented hydrogen at C-3 of a 3β-hydroxy triterpene. The geminal proton of the exocyclic double was observed at δ_H 4.58 and, 4.68. This characteristic suggests that **3** was a triterpene derivative. Moreover, the ¹³C-NMR and DEPT-135 spectrum of compound **3** as in Table 1 showed 30 carbon signals, six methyl's, twelve methylene, six methines, and six quaternary carbons confirming its pentacyclic triterpene skeleton. The signals at δ_C 60.8 and 79.2 indicate the presence of methine and methylene carbon of oxygenated hydroxy group (OH) at C-28 and C-3. The olefinic exocyclic carbon peaks assigned to C-29 and C-20 were exhibited at δ_C 109.8 and 150.3 respectively. Moreover, ¹H-¹H COSY spectrum showed correlations peaks between H-6/H-5, H-3/H-2, H-19/H-18, H-11/H-12, and H-29b/H-30. In addition, the HMBC spectrum also confirmed the correlation between H-15/C-13, H-30/C-29, H-3/C-24, H-18/C-20, H-9/C-26, H-18/C-20, H-30/C-20, and H-28/C-22, such correlation suggests that the isolated compound is pentacyclic triterpenoids. From the information received and the literature [22], it has been established that compound **3** is identified as betulin.

β-Hematin Polymerization Inhibition

Hematin Polymerization Inhibition Assay (HPIA) is a simple, reproducible, and inexpensive *in vitro* micro

assay [23]. Polymerization of hematin is a process that enables the detoxification of heme by the parasites because of haemoglobin degradation following its release in the lysosomal food vacuole [29]. *Plasmodium* passes through many stages throughout its life cycle, including an intraerythrocytic stage where the parasite breaks down 60-80% of the host's haemoglobin, which it uses as food for growth and development [30]. Within the parasite digestive vacuole, haemoglobin is oxidized to methaemoglobin and then degraded by aspartic proteases into free heme (Fe³⁺) (ferriprotoporphyrin IX) and denatured globin. Globin is hydrolysed into small peptides and amino acids required for protein synthesis by cysteine proteases [31]. During the process, Parasite detoxifies free heme through the formation of hemozoin (β-hematin) pigment. Hemozoin pigment is exhibited as a dark black crystalline spot or a dark brown pigment, which is physically and chemically identical to β-hematin. Hence, the best strategy to control malaria infections is by inhibiting its hemozoin formation, degradation of free heme by H₂O₂, and heme-binding proteins [4]. Chloroquine and other anti-malarial drugs have been reported to inhibit parasite growth by binding to hematin leading to the death of the parasite by hematin poisoning [32].

In this study, the *in vitro* anti-malarial assay was performed using the HPIA assay protocols. Three isolated compounds were investigated for this HPIA assay, namely lupenone (**1**), lupeol (**2**) and betulin (**3**). To assess the quality of the assay, the drug chloroquine was employed as a positive control. According to Baelmans *et al.*, tested compounds are only considered active for HPIA if their IC₅₀ value is below that of chloroquine sulphate positive control [33]. Therefore, for this assay, compounds **2** and **1** are considered active in comparison with the chloroquine IC₅₀ value as shown in Table 2. Based on the result obtained in this assay, it has been confirmed compounds **2** and **1** were considered active for the HPIA as their IC₅₀ values are all below the IC₅₀ value of chloroquine sulphate positive control. As presented in Table 2. Compound **2** is the most active compound with an IC₅₀ value of 20.2 ± 17 μM followed by compound **1** with an IC₅₀ value of 27.5 ± 23 μM lower than the IC₅₀ value of 37.5 ± 0.6 μM of chloroquine sulphate. However, compound **3** is considered moderate for this assay, having a higher IC₅₀ value of 40.9 ± 22 μM above the IC₅₀ value of 37.5 ± 0.6 μM of chloroquine (control).

Table 2. β-hematin polymerisation inhibition assay of compounds 1-3.

Compound	IC ₅₀ (μM)
Lupenone (1)	27.5 ± 23
Lupeol (2)	20.2 ± 17
Betulin (3)	40.9 ± 22
Chloroquine (Control)	37.5 ± 0.6
Mean ± Standard Deviation	

Molecular Docking

In silico molecular docking simulations were performed on the supercell crystal surfaces of β -hematin, also known as hemozoin using Autodock Vina for ligands **1-3** and the positive control chloroquine. This study was a seamless extension of the *in vitro* HPIA assay, aiming to further explore the binding characteristics. The interaction of the ligand with the crystal surface of hemozoin inhibited its further polymerisation, creating a toxic environment for the *Plasmodium sp.* parasite that subsequently killed it. The binding energy of ligands from docking

analysis are tabulated in Table 3.

Each of the examined ligands, namely **1**, **2**, and **3**, exhibited affinities ranging from -8.6 to -9.7 kcal mol⁻¹, while chloroquine recorded an affinity of -7.7 kcal mol⁻¹. The binding energies of the tested ligands, including the positive control, were all below -5 kcal mol⁻¹, signifying favourable interactions between the ligands and hemozoin [34]. The ligand-hemozoin binding interactions of **1-3** and chloroquine are tabulated in Table 4. The structure with the ring labelling of β -hematin, lupine-type triterpenoid and chloroquine are shown below in Figure 2 for the interactions reference.

Table 3. *In silico* binding energy of ligands **1-3** and positive control with hemozoin crystal.

Ligand	Binding energy (kcal mol ⁻¹)
Lupenone (1)	-8.6 ± 0.2
Lupeol (2)	-9.7 ± 0.1
Betulin (3)	-9.2 ± 0.1
Chloroquine (control)	-7.7 ± 0.3

Mean \pm standard deviation for n=3 experiments

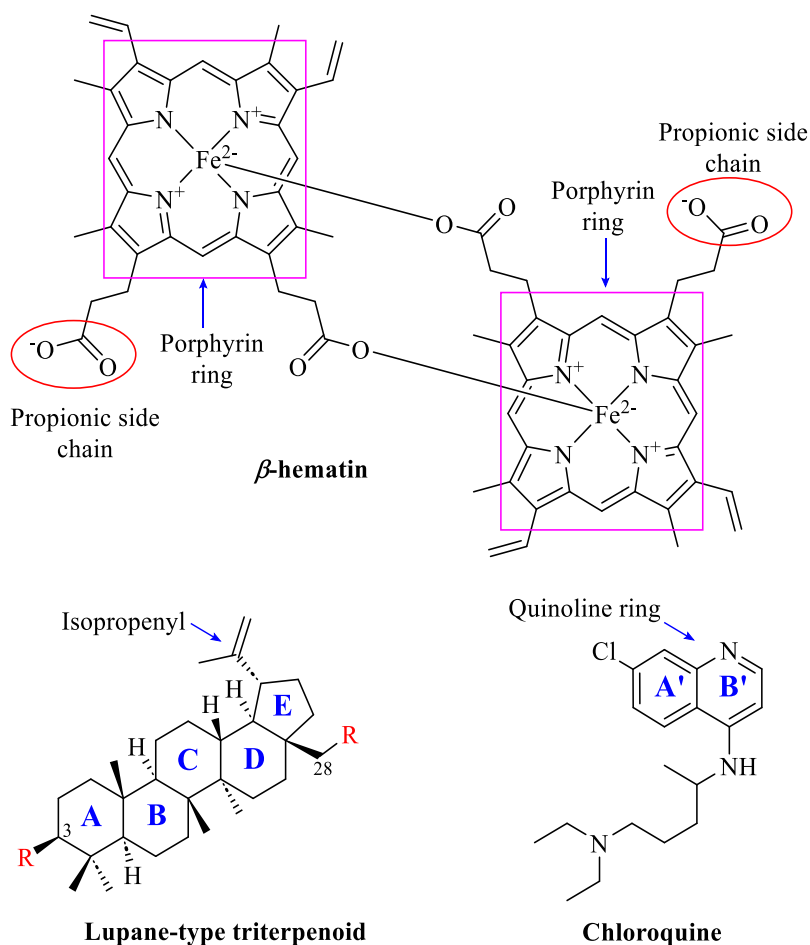


Figure 2. The chemical structures of β -hematin, lupane-type triterpenoid and chloroquine (control) with ring labelling for ligand-hemozoin interactions reference.

Table 4. Binding interactions between ligands 1-3 and chloroquine with hemozoin crystal.

Ligand	Interacting unit of ligand	Interacting unit of hemozoin	Type of interaction	Distance (Å)
(1)	-CH ₂ (Isopropenyl)	-CH ₂	Alkyl	4.06
	-CH ₂ (Isopropenyl)	-CH ₂	Alkyl	4.49
	-CH ₂ (Isopropenyl)	-CH ₂	Alkyl	4.10
	-CH ₂ (Isopropenyl)	Porphyrin ring	Pi-alkyl	4.29
	-CH ₂ (Isopropenyl)	Porphyrin ring	Pi-alkyl	4.53
	-CH ₃	-CH ₂	Alkyl	4.46
	-CH ₃	-CH ₂	Alkyl	4.49
	-CH ₃	-CH ₂	Alkyl	3.72
	-CH ₃	-CH ₂	Alkyl	3.67
	-CH ₃	-CH ₂	Alkyl	3.98
	-CH ₃	-CH ₂	Alkyl	4.44
	-CH ₃	-CH ₂	Alkyl	4.01
	-CH ₃	-CH ₂	Alkyl	4.43
	-CH ₃	-CH ₂	Alkyl	4.10
	-CH ₃	Porphyrin ring	Pi-alkyl	4.90
	Ring B	-CH ₂	Alkyl	4.86
	Ring B	Porphyrin ring	Pi-alkyl	5.49
	Ring C	-CH ₂	Alkyl	4.79
	Ring C	-CH ₂	Alkyl	5.28
	Ring D	-CH ₂	Alkyl	3.97
Ring D	-CH ₂	Alkyl	3.70	
Ring D	-CH ₂	Alkyl	4.96	
Ring E	-CH ₂	Alkyl	4.64	
Ring E	-CH ₂	Alkyl	4.31	
Ring E	-CH ₂	Alkyl	5.44	
(2)	-CH ₂ (Isopropenyl)	-CH ₂	Alkyl	4.27
	-CH ₂ (Isopropenyl)	Porphyrin ring	Pi-alkyl	4.89
	-CH ₂ (Isopropenyl)	Porphyrin ring	Pi-alkyl	4.08
	-CH ₂ (Isopropenyl)	Porphyrin ring	Pi-alkyl	3.65
	-CH ₃	-CH ₃	Alkyl	3.61
	-CH ₃	-CH ₂	Alkyl	3.96
	-CH ₃	-CH ₂	Alkyl	3.74
	-CH ₃	Porphyrin ring	Pi-alkyl	5.04
	-CH ₃	Porphyrin ring	Pi-alkyl	5.32
	-CH ₃	Porphyrin ring	Pi-alkyl	5.19
	-CH ₃ (Isopropenyl)	-CH ₂	Alkyl	3.83
	-CH ₃ (Isopropenyl)	-CH ₂	Alkyl	4.00
	-CH ₃ (Isopropenyl)	Porphyrin ring	Pi-alkyl	4.43
	-CH ₃ (Isopropenyl)	Porphyrin ring	Pi-alkyl	4.66
	-CH ₃ (Isopropenyl)	Porphyrin ring	Pi-alkyl	3.93
	-CH ₃ (Isopropenyl)	Porphyrin ring	Pi-alkyl	4.04
	Ring C	-CH ₂	Alkyl	4.77
	Ring C	Porphyrin ring	Pi-alkyl	5.43
	Ring D	-CH ₃	Alkyl	5.29
	Ring D	-CH ₂	Alkyl	3.66
	Ring D	-CH ₂	Alkyl	4.58
	Ring D	Porphyrin ring	Pi-alkyl	4.77
	Ring E	-CH ₂	Alkyl	4.61
Ring E	-CH ₃	Alkyl	3.63	
Ring E	-CH ₂	Alkyl	4.85	

	Ring E	-CH ₂	Alkyl	4.62
	Ring E	-CH ₂	Alkyl	5.47
	Ring E	Porphyrin ring	Pi-alkyl	4.55
	Ring E	Porphyrin ring	Pi-alkyl	3.80
Betulin (3)	C (CH ₂ OH)	O (Propionic side chain)	Carbon hydrogen bond	3.20
	-CH ₂ (Isopropenyl)	-CH ₂	Alkyl	4.09
	-CH ₂ (Isopropenyl)	Porphyrin ring	Pi-alkyl	4.86
	-CH ₂ (Isopropenyl)	Porphyrin ring	Pi-alkyl	4.14
	-CH ₂ (Isopropenyl)	Porphyrin ring	Pi-alkyl	3.58
	-CH ₃	-CH ₂	Alkyl	3.93
	-CH ₃	-CH ₂	Alkyl	3.59
	-CH ₃	Porphyrin ring	Pi-alkyl	5.20
	-CH ₃	Porphyrin ring	Pi-alkyl	5.00
	-CH ₃ (Isopropenyl)	-CH ₂	Alkyl	3.78
	-CH ₃ (Isopropenyl)	-CH ₂	Alkyl	3.87
	-CH ₃ (Isopropenyl)	Porphyrin ring	Pi-alkyl	4.34
	-CH ₃ (Isopropenyl)	Porphyrin ring	Pi-alkyl	4.53
	-CH ₃ (Isopropenyl)	Porphyrin ring	Pi-alkyl	4.00
	-CH ₃ (Isopropenyl)	Porphyrin ring	Pi-alkyl	4.07
	Ring C	-CH ₂	Alkyl	4.65
	Ring D	-CH ₂	Alkyl	3.63
	Ring D	-CH ₂	Alkyl	4.80
	Ring D	Porphyrin ring	Pi-alkyl	4.79
	Ring E	-CH ₂	Alkyl	4.48
	Ring E	-CH ₃	Alkyl	3.59
	Ring E	-CH ₂	Alkyl	4.94
	Ring E	-CH ₂	Alkyl	4.74
	Ring E	Porphyrin ring	Pi-alkyl	4.44
	Ring E	Porphyrin ring	Pi-alkyl	3.81
Chloroquine (Control)	C (Diethylamino)	O (Propionic side chain)	Carbon hydrogen bond	3.55
	Cl	-CH ₃	Alkyl	4.32
	Cl	-CH ₂	Alkyl	4.07
	Cl	-CH ₂	Alkyl	3.62
	Cl	Porphyrin ring	Pi-alkyl	3.61
	Cl	Porphyrin ring	Pi-alkyl	4.46
	-NH (Diethylamino)	O (Propionic side chain)	Conventional hydrogen bond	1.87
	Ring A'	Porphyrin ring	Pi-pi stacked	4.78
	Ring A'	Porphyrin ring	Pi-pi stacked	4.43
	Ring A'	Porphyrin ring	Pi-pi stacked	5.74
	Ring A'	Porphyrin ring	Pi-pi stacked	3.78
	Ring A'	-CH ₂	Pi-alkyl	4.97
	Ring A'	-CH ₂	Pi-alkyl	4.66
	Ring A'	-CH ₂	Pi-alkyl	4.70
	Ring B'	Porphyrin ring	Pi-pi stacked	4.03
	Ring B'	Porphyrin ring	Pi-pi stacked	4.18
	Ring B'	Porphyrin ring	Pi-pi stacked	4.55
	Ring B'	-CH ₃	Pi-alkyl	4.21
	Ring B'	-CH ₂	Pi-alkyl	5.22
	Ring B'	-CH ₂	Pi-alkyl	5.21

Ligand **1** exhibited a binding energy of 8.6 ± 0.2 kcal mol⁻¹ while binding to the (100) face of the hemozoin crystal. This interaction involved the formation of multiple hydrophobic interactions between them (Figure 3). The methylene groups of isopropenyl in **1** interacted with the methylene and porphyrin rings of hemozoin via hydrophobic alkyl and pi-alkyl interactions, respectively. The methyl groups attached to the lupane-type skeleton formed nine hydrophobic alkyl interactions with the methylene and one hydro-phobic pi-alkyl interaction with the porphyrin ring. In addition, ring B of **1** had one hydrophobic pi-alkyl interaction with the porphyrin ring and another hydro-phobic alkyl interaction with methylene. It was observed that rings C, D and E of **1** formed several hydrophobic alkyl interactions also with methylene from the hemozoin structure.

In the case of ligand **2**, it interacted with the (001) face of the hemozoin crystal, exhibiting a binding energy of -9.7 ± 0.1 kcal mol⁻¹ and engaging in multiple hydrophobic interactions with the receptor (Figure 4). Ligand **2** showed the highest potency among the isolated compounds tested for *in vitro* assay with an IC₅₀ of 20.2 ± 17 μM. The methyl and methylene groups of **2** interacted with the methylene and porphyrin rings of hemozoin via hydrophobic alkyl and hydrophobic pi-alkyl interactions. In addition, the methyl from the skeleton of **2** interacted with the methyl, methylene and porphyrin rings of the crystal receptor via another hydrophobic alkyl and pi-alkyl. Rings C, D, and E of **2** also had

multiple hydrophobic alkyl and pi-alkyl interactions with the methyl, methylene, and porphyrin rings, further supporting its binding to the hemozoin. Furthermore, ligand **3** possessed almost similar ligand-hemozoin interactions as **1** and **2**, with a slight addition of a carbon-hydrogen bond (3.20 Å) between the carbon (C-28) of **3** and the oxygen in the propionic acid side chain and docked to the (001) face of the hemozoin crystal (Figure 5).

In contrast to the most potent positive control, chloroquine (IC₅₀: 37.5 ± 0.6 μM) exhibited docking to the (001) face with a binding energy of -7.7 ± 0.3 kcal mol⁻¹. Chloroquine managed to sustain several distinct interactions when compared to the previously mentioned ligand (Figure 6). The -NH group and the carbon in the diethylamino moiety of chloroquine formed a conventional hydrogen bond (1.87 Å) and a carbon-hydrogen bond (3.55 Å) with the oxygen of the propionic side chain of hemozoin. The chlorine of chloroquine also interacted with the methyl, methylene, and porphyrin rings via hydrophobic alkyl and pi-alkyl interactions. The preferential interactions of the ligand-heme adduct known as hydrophobic pi-pi stacked [27, 35] were also shown between the A' and B' rings of chloroquine and the porphyrin ring of hemozoin, with a total of seven interactions registered. The binding between chloroquine and hemozoin was further enhanced by the interaction between rings A' and B' with the methyl and methylene units of the receptor through hydrophobic pi-alkyl interactions. The interactions described above provide insight into why chloroquine, a drug utilized as an anti-malarial agent, exhibits significant effectiveness.

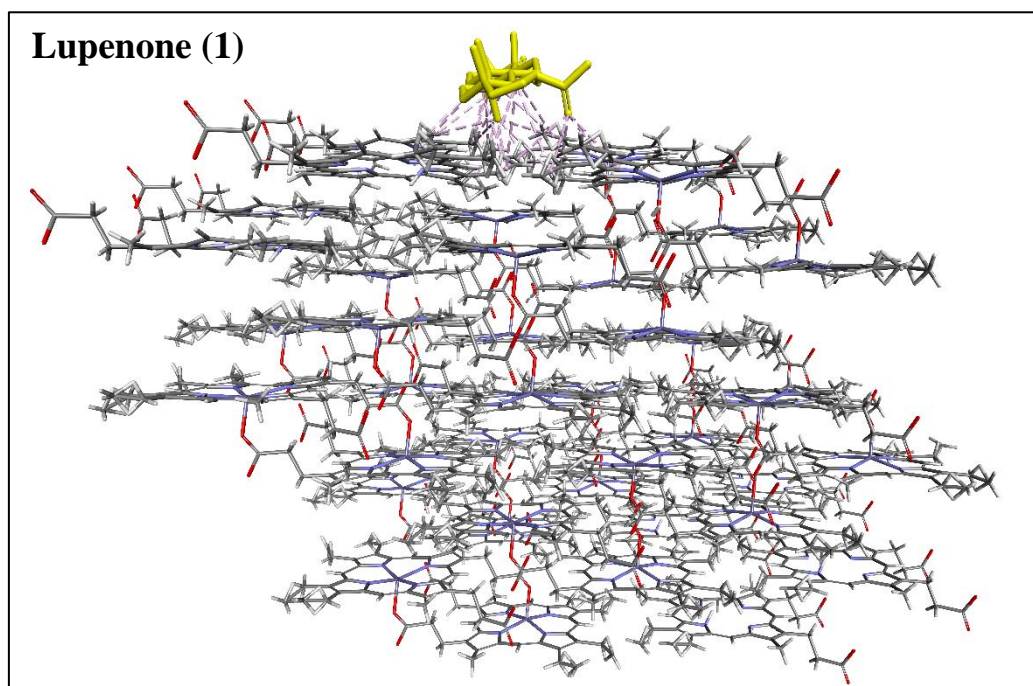


Figure 3. Docked conformation of hemozoin crystal with **1**.

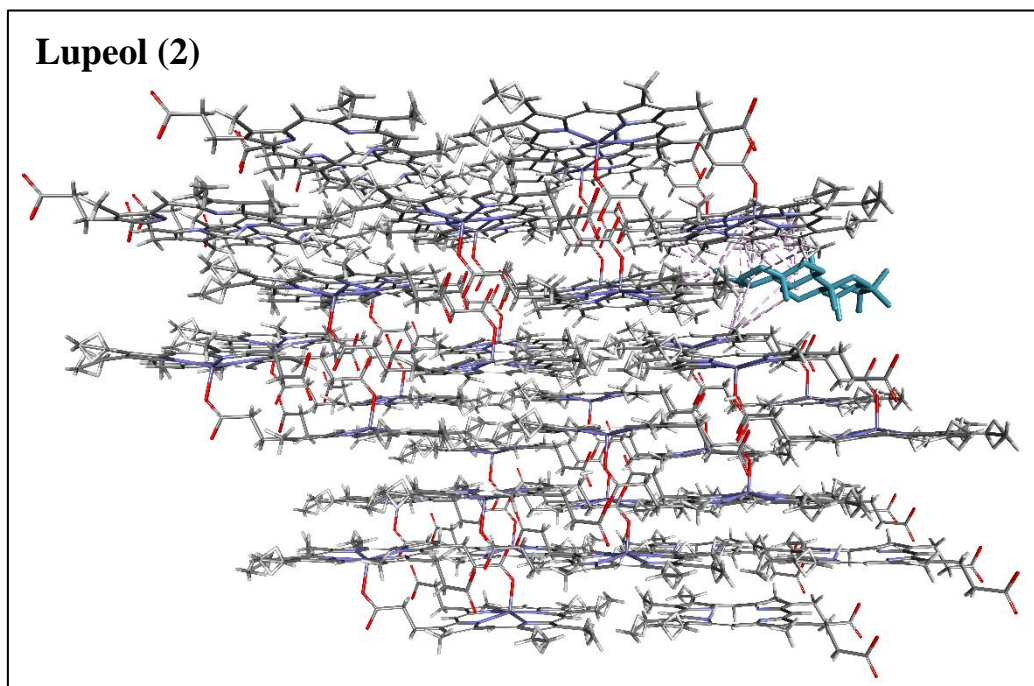


Figure 4. Docked conformation of hemozoin crystal with 2.

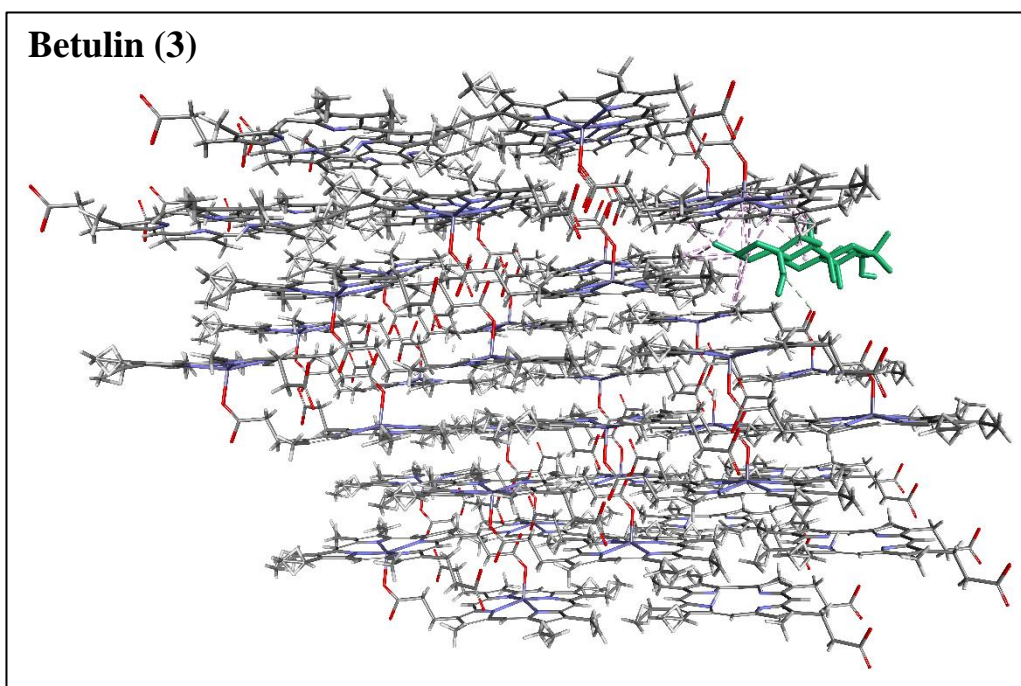


Figure 5. Docked conformation of hemozoin crystal with chloroquine.

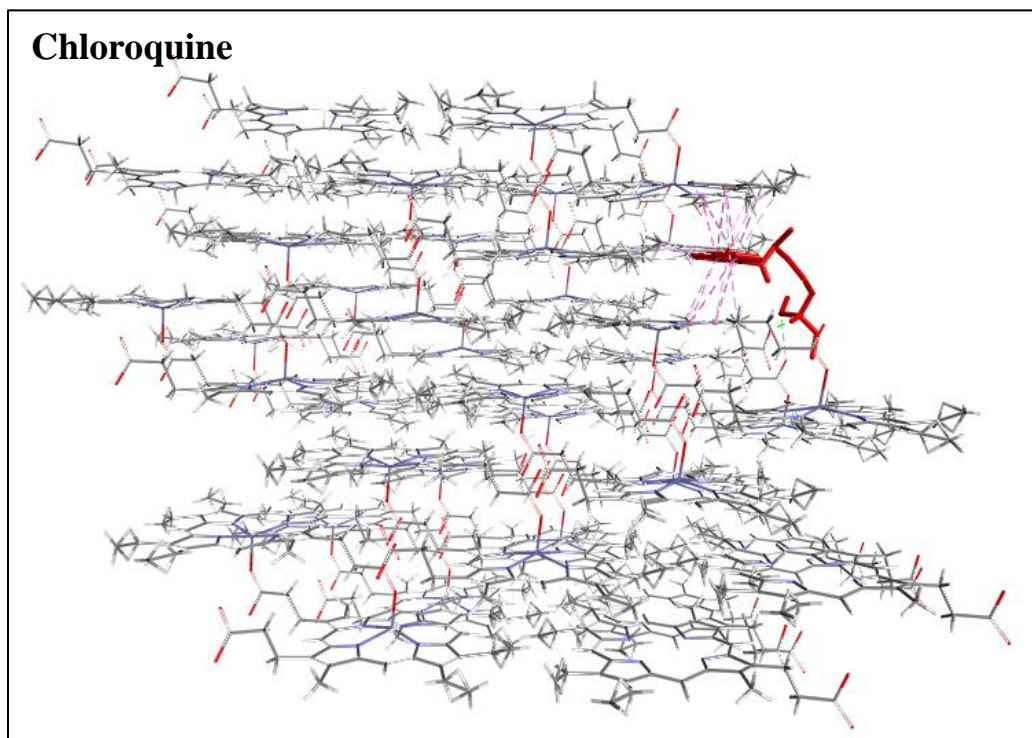


Figure 6. Docked conformation of hemozoin crystal with chloroquine.

CONCLUSION

As a summary, three compounds [i.e. lupenone (**1**), lupeol (**2**) and betulin (**3**)] were isolated from the bark of *D. Adenophora*. Their structure was elucidated using various spectroscopic techniques and the compounds were identified as pentacyclic triterpenes when compared with reported literature. The compounds were evaluated *in vitro* anti-malarial activity on β -hematin polymerization inhibition and a molecular docking study. Among them, compounds **1** and **2** show a good inhibition (20-27 μM) in comparison to the positive control, chloroquine ($\text{IC}_{50} = 37.5 \pm 0.6 \mu\text{M}$). In the examination of ligand binding to the hemozoin crystal, ligand **2** and chloroquine both demonstrated interactions with the (001) face of hemozoin involving hydrophobic interactions. While both ligands shared this commonality, ligand **2** exhibited a notably stronger binding affinity with a binding energy of $-9.7 \pm 0.1 \text{ kcal mol}^{-1}$, whereas chloroquine displayed a binding energy of $-7.7 \pm 0.3 \text{ kcal mol}^{-1}$, indicating ligand **2**'s enhanced binding strength. Chloroquine's interactions extended to include hydrogen and carbon-hydrogen bonds with the propionic side chain of hemozoin, distinctions not found in ligand **2**'s interactions. Despite ligand **2**'s stronger binding energy, chloroquine demonstrated higher potency in inhibiting hemozoin formation with an IC_{50} of $37.5 \pm 0.6 \mu\text{M}$, compared to ligand **2**'s IC_{50} of $20.2 \pm 17 \mu\text{M}$, which might be attributed to its additional hydrophobic pi-pi stacked interactions with hemozoin's porphyrin ring. These findings collectively underline the effectiveness of ligand **2**

and chloroquine as an anti-malarial agent, highlighting the importance of its diverse and potent interactions with hemozoin.

ACKNOWLEDGEMENTS

The authors would like to thank Universiti Sains Malaysia (USM) for the research facilities throughout the period of this research work. IDB acknowledges Umaru Ali Shinkafi Polytechnic for the sponsorship through Tertiary Education Trust Fund (TETFUND). This research was conducted within the frame of the collaboration between USM-CNRS (MoU) and auspices of CNRS-UM; Associated International Laboratory (LIA) under FM-NatProLab. We thank Din M.N., Rafly S. and Teo L.E. (UM) for the collection and identification of plant material.

REFERENCES

1. Mosaddegh, M., Irani, M. & Esmaili, S. (2018) Inhibition test of heme detoxification (ITHD) as an approach for detecting antimalarial agents in medicinal plants. *Research Journal of Pharmacognosy*, **5**, 5–11.
2. Olanlokun, J. O., Adetutu, J. A. & Olorunsogo, O. O. (2021) *In vitro* inhibition of beta-hematin formation and *in vivo* effects of *Diospyros mespiliformis* and *Mondia whitei* methanol extracts on chloroquine-susceptible *Plasmodium berghei*-induced malaria in mice. *Interventional Medicine and Applied Science*, **11**, 197–206.

- 132 Ibrahim Dankane Bafarawa, Muhammad Solehin Abd Ghani, Mohamad Nurul Azmi, Arba Pramundita Ramadani, Dian Nida Salsabila, Arde Toga Nugraha, Sista Werdyani, Muhammad Bisyrul Hafi Othman, Mohammad Nasir Ibrahim, Khalijah Awang, Marc Litaudon, and Mohammad Tasyriq Che Omar
3. Nyandwaro, K., Oyweri, J., Kimani, F. & Mbugua, A. (2020) Evaluating antiplasmodial and anti-malarial activities of soybean (*Glycine max*) seed extracts on *P. falciparum* parasite cultures and *P. berghei*-infected mice. *Journal of Pathogens*, **2020**, 1–8.
4. Mohebi, M., Fayazi, N., Esmaeili, S., Rostami, M., Bagheri, F., Aliabadi, A. & Saghaie, L. (2022) Synthesis, characterization, molecular docking, antimalarial, and antiproliferative activities of benzyloxy-4-oxopyridin benzoate derivatives. *Research in Pharmaceutical Sciences*, **17**, 252–264.
5. Pan, W. H., Xu, X. Y., Shi, N., Tsang, S. W. & Zhang, H. J. (2018) Antimalarial activity of plant metabolites. *International Journal of Molecular Sciences*, **19**, 1382–1422.
6. Newman, D. J. & Cragg, G. M. (2020) Natural products as sources of new drugs over the nearly four decades from 01/1981 to 09/2019. *Journal of Natural Products*, **83**, 770–803.
7. du Preez-Bruwer, I., Mumbengegwi, D. R. & Louw, S. (2022) *In vitro* antimalarial properties and chemical composition of *Diospyros chamaethamnus* extracts. *South African Journal of Botany*, **149**, 290–296.
8. Rauf, A., Uddin, G., Patel, S., Khan, A., Halim, S. A., Bawazeer, S. & Mubarak, M. S. (2017) *Diospyros*, an under-utilized, multi-purpose plant genus: A review. *Biomedicine and Pharmacotherapy*, **91**, 714–730.
9. Guo, D. L. & Luo, Z. R. (2011) Genetic relationships of the Japanese persimmon *Diospyros kaki* (Ebenaceae) and related species revealed by SSR analysis. *Genetic and Molecular Research*, **10**, 1060–1068.
10. Peyrat, L. A., Eparvier, V., Eydoux, C., Guillemot, J. C., Stien, D. & Litaudon, M. (2016) Chemical diversity and antiviral potential in the pantropical *Diospyros* genus. *Fitoterapia*, **112**, 9–15.
11. Rauf, A., Uddin, G., Siddiqui, B. S., Molnár, J., Csonka, Á., Ahmad, B., Szabó, D., Farooq, U. & Khan, A. (2015) A rare class of new dimeric naphthoquinones from *Diospyros lotus* have multi-drug reversal and antiproliferative effects. *Frontiers in Pharmacology*, **2015**, 1–9.
12. Das, S., Haldar, P. K., Pramanik, G., Panda, S. P. & Bera, S. (2011) Evaluation of analgesic and anti-inflammatory activity of *Diospyros cordifolia* extract. *African Journal of Traditional, Complementary and Alternative Medicines*, **8**, 11–14.
13. Wisetsai, A., Schevenels, F. T. & Lekphrom, R. (2021) Chemical constituents and their biological activities from the roots of *Diospyros filipendula*. *Natural Product Research*, **35**, 2739–2743.
14. Ayepola, O. O., Olasehinde, G. I., Adedeji, O. A., Adeyemi, O. O. & Onile-Ere, O. A. (2018) *In vitro* antimicrobial activity of crude extracts of *Diospyros monbuttensis*. *African Journal of Clinical and Experimental Microbiology*, **19**, 84–87.
15. Adzu, B., Amos, S., Dzarma, S., Muazzam, I. & Gamaniel, K. S. (2002) Pharmacological evidence favouring the folkloric use of *Diospyros mespiliformis* Hochst in the relief of pain and fever. *Journal of Ethnopharmacology*, **82**, 191–195.
16. Tameye, N. S. J., Akak, C. M., Happi, G. M., Frese, M., Stammer, H. G., Neumann, B., Lenta B. N., Sewald, N. & Nkengfack, A. E. (2020) Antioxidant norbergenin derivatives from the leaves of *Diospyros gillettii* De Wild (Ebenaceae). *Phytochemistry Letters*, **36**, 63–67.
17. Rathore, K., Singh, V. K., Jain, P., Rao, S. P., Ahmed, Z. & Singh, V. D. (2014) *In-vitro* and *in-vivo* antiadipogenic, hypolipidemic and antidiabetic activity of *Diospyros melanoxylon* (Roxb). *Journal of Ethnopharmacology*, **155**, 1171–1176.
18. Ruphin, F. P., Baholy, R., Emmanuel, R., Amelie, R., Martin, M. T. & Koto-te-Nyiwa, N. (2014) Isolation and structural elucidation of cytotoxic compounds from the root bark of *Diospyros quercina* (Baill.) endemic to Madagascar. *Asian Pacific Journal of Tropical Biomedicine*, **4**, 169–175.
19. Feusso, H. M. F., Dongmo, J. D. D., Djomkam, H. L. M., Akak, C. M., Lateef, M., Ahmed, A., Azebaze, A. G. B., Waffo, A. F. K., Ali, M. S. & Vardamides, J. C. (2020) Chemicals constituents from leaves of *Diospyros iturenensis* (Gürke) Letouzey & F. White and their biological activities. *Natural Product Sciences*, **26**, 311–316.
20. Duong, H. T. (2019) A further investigation on the chemical constituents from *Euphorbia tirucalli* growing in Binh Thuan province. *VNUHCM Journal of Science and Technology Development*, **22**, 247–252.
21. Shwe, H. H., Win, K. K., Moe, T. T., Myint, A. A. & Win, T. (2019) Isolation and structural characterization of lupeol from the stem bark of *Diospyros ehretioides* Wall. *IEEE-SEM*, **7**, 140–144.
22. Tijjani, A., Ndukwe, I. G. & Ayo, R. G. (2012) Isolation and characterization of lup-20 (29)-ene-3, 28-diol (Betulin) from the stem bark of

- 133 Ibrahim Dankane Bafarawa, Muhammad Solehin Abd Ghani, Mohamad Nurul Azmi, Arba Pramundita Ramadani, Dian Nida Salsabila, Arde Toga Nugraha, Sista Werdyani, Muhammad Bisyrul Hafi Othman, Mohammad Nasir Ibrahim, Khalijah Awang, Marc Litaudon, and Mohammad Tasyriq Che Omar
- Isolation, Characterization, Molecular Docking, and Antimalarial Activity of Chemical Constituents of *Diospyros adenophora*.
- Adenium obesum* (Apocynaceae). *Tropical Journal of Pharmaceutical Research*, **11**, 259–262.
23. Basilio, N., Pagani, E., Monti, D., Olliaro, P. & Taramelli, D. (1998) A microtitre-based method for measuring the haem polymerization inhibitory activity (HPIA) of antimalarial drugs. *The Journal of Antimicrobial Chemotherapy*, **42**, 55–60.
24. Morris, G. M. & Lim-Wilby, M. (2008) Molecular docking. In *Methods Molecular Biology, Humana Press*, **443**, 365–382.
25. Trott, O. & Olson, A. J. (2010) AutoDock Vina: Improving the speed and accuracy of docking with a new scoring function, efficient optimization, and multithreading. *Journal of Computational Chemistry*, **31**, 455–461.
26. Eberhardt, J., Santos-Martins, D., Tillack, A. F. & Forli, S. (2021) AutoDock Vina 1.2.0: New docking methods, expanded force field, and python bindings. *Journal of Chemical Information and Modeling*, **61**, 3891–3898.
27. Jilani, N. A. K., Oka, N., Ando, K. & Hasbullah, S. A. (2023) Synthesis, characterisation and binding evaluation of new 6-amidinoindole compound as the potential heme binder. *Sains Malaysiana*, **52**, 1231–1242.
28. Momma, K. & Izumi, F. (2011) VESTA 3 for three-dimensional visualization of crystal, volumetric and morphology data. *Journal of Applied Crystallography*, **44**, 1272–1276.
29. Kurosawa, Y., Dorn, A., Kitsuji-Shirane, M., Shimada, H., Satoh, T., Matile, H., Hofheinz, W., Masciadri, R., Kansy, M. & Ridley, R. G. (2000) Hematin polymerization assay as a high-throughput screen for identification of new antimalarial pharmacophores. *Antimicrobial Agents and Chemotherapy*, **44**, 2638–2644.
30. Ridley, R. G., Dorn, A., Vippagunta, S. R. & Vennerstrom, J. L. (1997) Haematin (haem) polymerization and its inhibition by quinoline antimalarials. *Annals of Tropical Medicine & Parasitology*, **91**, 559–566.
31. Herraiz, T., Guillén, H., González-Peña, D. & Arán, V. J. (2019) Antimalarial quinoline drugs inhibit β -hematin and increase free hemin catalyzing peroxidative reactions and inhibition of cysteine proteases. *Scientific Reports*, **9**, 15398.
32. Rosenthal, P. J. (2003) Antimalarial drug discovery: old and new approaches. *Journal of Experimental Biology*, **206**, 3735–3744.
33. Ecker, A., Lehane, A. M., Clain, J. & Fidock, D. A. (2012) PfCRT and its role in antimalarial drug resistance. *Trends in Parasitology*, **28**, 504–514.
34. Takahashi, O., Masuda, Y., Muroya, A. & Furuya, T. (2010) Theory of docking scores and its application to a customizable scoring function. *SAR and QSAR in Environmental Research*, **21**, 547–558.
35. Veale, C. G., Jayram, J., Naidoo, S., Laming, D., Swart, T., Olivier, T., Akerman, M. P., de Villiers, K. A., Hoppe, H. C. & Jeena, V. (2020) Insights into structural and physicochemical properties required for β -hematin inhibition of privileged triarylimidazoles. *RSC Medicinal Chemistry*, **11**, 85–91.